JPCCCK

APRIL 14, 2011
VOLUME 115
NUMBER 14
pubs.acs.org/JPCC

THE JOURNAL OF PHYSICAL CHEMISTRY C

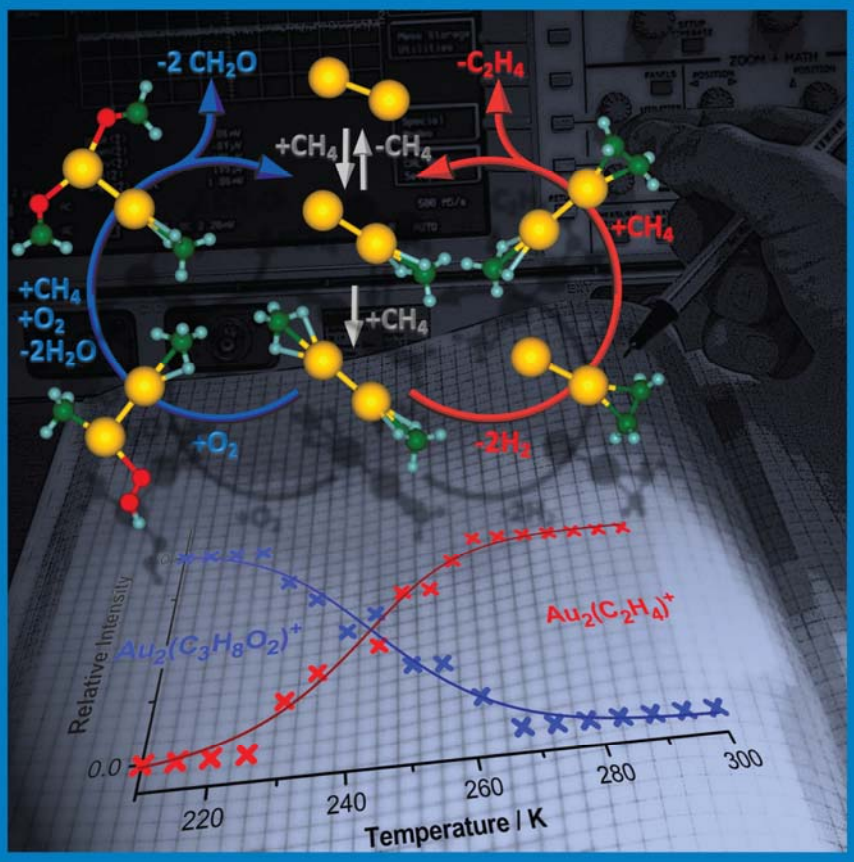

Low- (Blue) and High- (Red) Temperature Au_2^+-Catalyzed Methane Activation Selective Reaction Cycles
(see page 5A)

NANOMATERIALS, INTERFACES, HARD MATTER

CAPTION

Low- (blue) and high- (red) temperature Au_2^+-catalyzed methane activation selective reaction cycles. Reaction kinetics and mass spectrometry radio frequency trap experiments in conjunction with first-principles density functional theory simulations reveal that gold dimer cations catalyze temperature-tuned selective reactions in gaseous mixtures of oxygen and methane. Temperature-controlled catalytic selectivity is demonstrated through the conversion of a mixture of methane and oxygen to formaldehyde at temperatures below 250 K (left catalytic cycle, blue color), while at higher temperatures (up to 300 K) dehydrogenation processes lead predominantly to formation of ethylene (right catalytic cycle, red color). On the bottom chart, we display the measured relative intensities of the catalyzed reaction products plotted versus the reaction temperature. Microscopic mechanisms were predicted theoretically and tested against the measured data. The corresponding molecular structures of the reaction intermediates and products are superimposed on the reaction cycles. Gold atoms are depicted by yellow spheres, oxygen atoms are in red, carbon atoms are in green, and hydrogen atoms are described by small blue spheres. See page 6788. View the article.

THE JOURNAL OF PHYSICAL CHEMISTRY C

ARTICLE

pubs.acs.org/JPCC

Temperature-Tunable Selective Methane Catalysis on Au_2^+: From Cryogenic Partial Oxidation Yielding Formaldehyde to Cold Ethylene Production

Sandra M. Lang,[†] Thorsten M. Bernhardt,[†] Robert N. Barnett,[‡] and Uzi Landman*[,‡]

[†]Institute of Surface Chemistry and Catalysis, University of Ulm, Albert-Einstein-Allee 47, 89069 Ulm, Germany

[‡]School of Physics, Georgia Institute of Technology, Atlanta, Georgia 30332-0430, United States

ABSTRACT: The catalytic partial oxidation of methane into valuable products is of great scientific importance and considerable industrial and economical interest. Particularly challenging is the direct and selective oxidation of methane with molecular oxygen at moderate temperatures in a "green", sustainable, and ecological manner. A mixture of methane and molecular oxygen is shown to selectively convert into formaldehyde at temperatures below 250 K if mass-selected Au_2^+ clusters are introduced into the gas mixture as catalysts. At higher temperatures O_2 does not adsorb readily on the gold clusters, and catalyzed cooperative dehydrogenation of methane molecules results in the formation of ethylene. Gas-phase reaction kinetics measurements in a radio frequency ion trap under multicollision conditions, in conjunction with first-principles simulations, reveal mechanistic details of the temperature-tunable coupled catalytic cycles. The discovery of temperature-controlled dehydrogenation/partial-oxidation selective catalytic cycles is an important step in the rational design of gold-based low temperature oxidation catalysts.

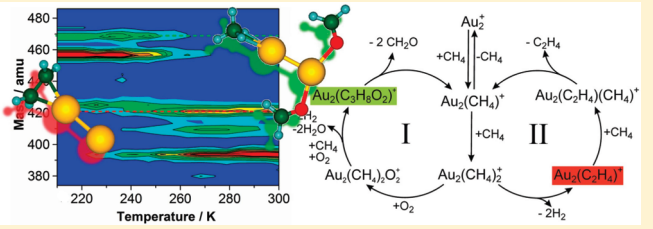

1. INTRODUCTION

Methane gas is a key feedstock in the modern technological society, and it is abundantly available from fossil or biogenic sources. In addition to its utilization in combustion, the activation of the methane molecule and its catalytic conversion into more valuable products like methanol, formaldehyde, or ethylene is highly desirable. Although extensive research has been devoted to the selective partial oxidation of methane at both elevated and ambient temperature and pressure conditions, no efficient selective synthesis route for methane activation and conversion has been devised as of yet.[1−3] A problem that emerges in the course of searching for highly active catalytic materials capable of activating the stable C−H bonds of methane pertains to the finding that such highly reactive catalysts generally yield little selectivity with respect to the subsequently formed products and often even lead to complete combustion.[1,4]

The future development of suitable catalytic materials that would overcome these limitations and facilitate the selective and direct methane oxidation under ambient and environmentally compatible conditions requires fundamental insight into the C−H bond activation and reaction processes at the molecular level. To this aim, the combined tools of gas-phase reaction experiments employing advanced mass spectrometry instrumentation and state-of-the-art first-principles theoretical simulations provide a powerful means for the determination and assessment of elementary mechanistic details of complex catalytic processes.[5−8]

Previous gas-phase investigations of the oxygenation of methane employing transition-metal oxides[9,10] or Pt^+ ions[10,11] as catalytically active species already led to the development of certain molecular level mechanistic concepts pertaining to methane activation. However, the earlier studies showed low oxidation product selectivity or the need to provide N_2O instead of O_2 as an oxidizing reagent.[5] On the other hand, gold nanoparticle-based catalysts,[12,13] as well as small free gold clusters,[7,8,14] have been shown to be able to activate molecular oxygen at low temperatures, thus presenting a primary choice in the quest for a sustainable oxidation chemistry.[12] In addition, the cooperative activation of CH_4 by the cationic gold dimer Au_2^+ was recently observed in a gas-phase radio frequency (rf) ion trap experiment under multicollision conditions.[6] In this gas-phase experiment, collision frequencies on the order of 10^5 s^{-1} are maintained inside the ion trap.[15] In addition to enabling temperature-dependent reaction kinetics measurements that provide detailed mechanistic insights, these conditions bridge the gap between ultrahigh vacuum single collision studies and practical high pressure catalysis.[3]

In the present contribution, the catalytic Au_2^+-mediated coupling of methane and molecular oxygen is investigated in such ion trap experiments. Mass spectrometric product analysis reveals the catalytic reaction of CH_4 with O_2 at temperatures below 250 K, and detailed first-principles calculations predict the selective formation of formaldehyde. At higher temperatures O_2

Received: January 6, 2011
Revised: February 7, 2011
Published: March 10, 2011

dx.doi.org/10.1021/jp200160r | J. Phys. Chem. C 2011, 115, 6788–6795

does not adsorb on Au_2^+, and the activated adsorbed methane molecules yield ethylene through cooperative dehydrogenation. Reaction kinetics measurements in conjunction with theoretical simulations allow the formulation and testing of two coupled product-selective catalytic cycles that are operatively temperature controlled. Details of the reaction profile, as well as the energetics, dynamics, and structures of the reaction intermediates and transition state complexes, are presented.

2. METHODS

2.1. Experimental Setup. The experimental setup to study the gold dimer reactions consists of a variable-temperature rf octopole ion trap inserted into a low energy ion beam assembly of two quadrupole mass spectrometers and two ion guides. The general experimental layout is described in detail elsewhere and will only be outlined briefly here.[15]

Metal cluster cations are produced by employing a CORDIS (cold reflex discharge ion source)[16] Xe ion source to simultaneously sputter four metal targets. The cluster ion beam is steered into a helium-filled quadrupole ion guide to collimate and thermalize the hot cluster ions before the gold dimer is mass-selected from the beam in an adjacent first quadrupole mass filter. The Au_2^+ ion beam is then transferred via a second quadrupole ion guide into the home-built octopole ion trap, which is prefilled with about 0.9 Pa of helium and small partial pressures of CH_4 and O_2. The absolute pressure inside the trap is measured by a Baratron capacitance manometer (MKS, Typ 627B). The ion trap is attached to a closed cycle helium cryostat that allows for temperature adjustment in the range between 20 and 300 K. Thermal equilibration of the clusters is achieved within a few milliseconds (about 10^3 collisions) under our experimental conditions,[15] while the clusters are stored for a considerably longer time, typically between 0.1 s and several seconds. After the chosen reaction, i.e., storage time t_R, all ionic reactants, intermediates, and products are extracted from the ion trap. The ion distribution is subsequently analyzed by a second quadrupole mass filter. To account for a slightly asymmetric mass peak shape occurring at very low ion intensities in our apparatus, the raw data have been deconvoluted with a constant apparatus function to yield the shown mass spectra.[17]

By recording all ion intensities as a function of the reaction time t_R the kinetics at a well-defined reaction temperature can be obtained. The normalized kinetic traces are then evaluated by fitting the integrated rate equations of potential reaction mechanisms to the experimental data by using the "Detmech" software.[18] This leads to the determination of the simplest reaction mechanism that best fits the experimental data. Because the experiments were performed around 1 Pa total pressure and thus in the kinetic low pressure regime, the details of every association reaction step can be described by the Lindeman energy transfer model for association reactions, while the details of every dissociation reaction step can be described by the Lindeman mechanism.[15,19,20]

2.2. Computational Methods. The theoretical explorations of the atomic arrangements and electronic structures of Au_2^+ and its complexes with the methane molecules along the reaction paths have been performed with the use of first-principles density functional theory (DFT) calculations. In particular, we employed the Born−Oppenheimer (BO)−spin density functional (SDF)−molecular dynamics (MD) method, BO−SDF−MD,[21] with norm-conserving soft pseudopotentials (including a scalar relativistic pseudopotential for Au)[22] and the generalized gradient approximation (GGA)[23] for electronic exchange and correlations. In these calculations we have used a plane-wave basis with a kinetic energy cutoff of 62 Ry. The BO−SDF−MD method is particularly suitable for investigations of charged systems since it does not employ a supercell (i.e., no periodic replication of the ionic system is used). Structural optimizations were performed using a conjugate-gradient-like method.

In the first-principles calculations of the reaction profiles (pathways), a reaction coordinate was judiciously chosen; the reaction coordinate may consist of several geometrical parameters pertinent for the studied mechanism—for example, a reaction coordinate may entail at a certain stage the distance between two reacting atoms, e.g., the distance between an H atom of an adsorbed methane molecule and the nearest Au atom—while at a subsequent stage of the reaction the pertinent reaction coordinate may correspond to the rotation angle of a chosen molecular group. For each value of the reaction coordinate, the total energy of the system was optimized through unconstrained relaxation of all of the other degrees of freedom of the system (reactant molecules and gold cluster atoms). The reaction profiles were obtained via repeating such calculations for various values of the chosen reaction coordinate. Moreover, alternative reaction pathways have been attempted and assessed through comparisons with the experimental data.

In the present study, we restricted ourselves to consideration of enthalpic effects on the reaction profile since for the range of temperatures investigated by us here (210−300 K) entropic effects are expected to be rather small (particularly for the relatively small molecular systems investigated here). Nevertheless, we note that free-energy reaction profiles (i.e., including entropic effects) can be obtained through canonical (constant-temperature) first-principle (Born−Oppenheimer) molecular dynamics (FPBOMD) simulations,[21] while constraining the reaction coordinate to prescribed values (see discussion in section 1.3.2, pp 87−90 in ref 13(d)). This process is repeated for a number of points along the reaction path, and the mean-force of constraint at these points is recorded. An integral of the mean force multiplied by the corresponding distance along the reaction coordinate (taken between two points selected along the reaction path) yields the reversible work done in taking the system along the reaction path between the two selected points; in the canonical ensemble this work equals the Helmholtz free-energy difference between the two points. This method is related to the thermodynamic integration method commonly employed in investigations of condensed phases and biophysical systems.

3. RESULTS

3.1. Experimental Results. In our experiment, the rf ion trap is filled with about 0.1 Pa partial pressures of CH_4 and O_2, respectively, in addition to ∼0.9 Pa of He buffer gas. Subsequently, a mass-selected beam of Au_2^+ is allowed to enter the ion trap, and the gold dimer ions are accumulated up to the space charge limit (∼10^7 ions per cm^3). Mass spectra of the ionic products in the trap are then recorded after chosen reaction times. Figure 1 displays examples of such product ion mass distributions together with the corresponding temporal product ion intensity evolutions (kinetic traces) at three selected temperatures.

At a temperature of 210 K (mass spectrum a in Figure 1), the products $Au_2(CH_4)_2^+$ (marked by the blue circle in Figure 1),

dx.doi.org/10.1021/jp200160r |J. Phys. Chem. C 2011, 115, 6788–6795

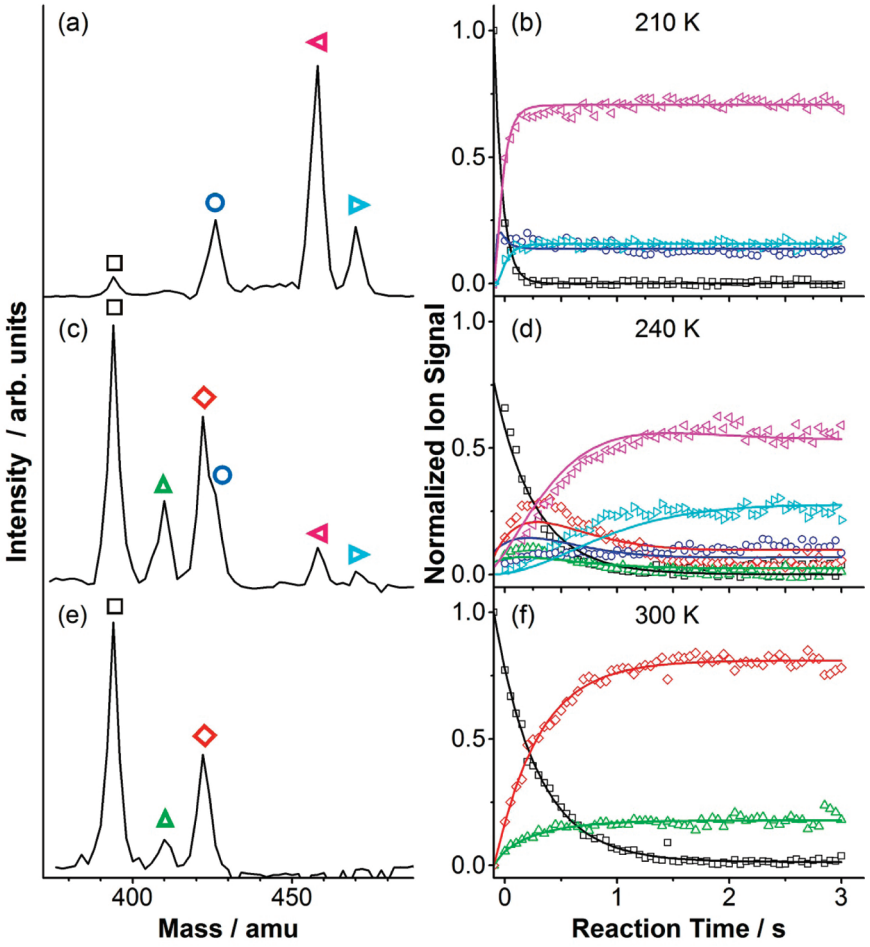

Figure 1. (a, c, e) Temperature-dependent mass spectra (recorded after 0.1 s reaction time) and (b, d, f) reaction kinetics obtained from the reaction between Au_2^+ and a mixture of CH_4 and O_2. (a) and (b) 210 K, $p(He) = 0.98$ Pa, $p(CH_4) = 0.03$ Pa, $p(O_2) = 0.05$ Pa; (c) and (d) 240 K, $p(He) = 0.85$ Pa, $p(CH_4) = 0.12$ Pa, $p(O_2) = 0.11$ Pa; (e) and (f) 300 K, $p(He) = 0.85$ Pa, $p(CH_4) = 0.06$ Pa, $p(O_2) = 0.11$ Pa. The open symbols in the kinetics represent the experimental data, normalized to the total ion concentration in the ion trap. The solid lines are obtained by fitting the integrated rate equations of the proposed reaction mechanism depicted in Figure 2c to the experimental data. Please note that a fragment signal, $Au(C_2H_4)(CH_4)^+$, which is formed to a minor extent above 250 K, is omitted here for to the sake of clarity.[6] The effect of the fragment on the kinetics is a slow overall decrease of all ion signal intensities with increasing reaction time. The peak labels correspond to: black □, Au_2^+; green △, $Au_2(CH_4)$; red ◇, $Au_2(C_2H_4)^+$; blue ○, $Au_2(CH_4)_2^+$; pink triangle pointing left, $Au_2(CH_4)_2O_2^+$; teal triangle pointing right, $Au_2(C_3H_8O_2)^+$.

$Au_2(CH_4)_2O_2^+$ (pink triangle pointing left), and $Au_2(C_3H_8O_2)^+$ (teal triangle pointing right) are detected, in addition to the pure gold dimer signal (black square). The most interesting observation is the detection of the oxygen-containing complexes $Au_2(CH_4)_2O_2^+$ and $Au_2(C_3H_8O_2)^+$, which is even more surprising because Au_2^+ does not form any reaction products with O_2 alone.[7] Therefore, the formation of both $Au_2(CH_4)_2O_2^+$ and $Au_2(C_3H_8O_2)^+$ results from cooperative effects of the methane preadsorption, suggesting that the third ion observed at this temperature, $Au_2(CH_4)_2^+$, is likely to be a precursor to these products (see our discussion of the inset to Figure 3c and Figure 4). A similar cooperative adsorption and activation of molecular oxygen on small Au_n^+ clusters has been previously observed to be promoted through hydrogen preadsorption.[7]

The stoichiometries of $Au_2(CH_4)_2O_2^+$ and $Au_2(C_3H_8O_2)^+$ have been confirmed by isotopoic labeling experiments with both deuterated methane and monoisotopic oxygen $^{18}O_2$. While $Au_2(CH_4)_2O_2^+$ might correspond to a simple coadsorption product of two methanes and one oxygen molecule, $Au_2(C_3H_8O_2)^+$ clearly contains activated and dehydrogenated methane indicating a possible C−O coupling reaction. However, based on the mass spectrometric measurements alone, the structures of these products cannot be assessed.

Further insight can be gained from the reaction kinetics obtained at this temperature (210 K), which is shown in Figure 1b. The product formation is fast under the given experimental conditions, and after less than 500 ms the Au_2^+ signal has disappeared. The intensities of $Au_2(CH_4)_2^+$, $Au_2(CH_4)_2O_2^+$, and $Au_2(C_3H_8O_2)^+$, however, attain nonvanishing saturated values in the kinetic data at longer reaction times. Such kinetic traces can only be explained by an equilibrium reaction mechanism (all products are connected with each other by forward and backward reaction steps) or by a reaction cycle.[19] However, due to the obvious methane dehydrogenation reaction accompanying the formation of $Au_2(C_3H_8O_2)^+$, an equilibrium reaction mechanism is physically not reasonable because the concentration of molecular hydrogen in the ion trap is far too low for the backward reaction to occur. Thus, the formation of the oxygen-containing products must occur as part of a catalytic reaction cycle.

The formulation of the details of this catalytic cycle has been guided by the results of our theoretical first-principles simulations. The simplest reaction mechanism that best fits the experimental data and which, based on our theoretical modeling (see discussion below), is considered the most likely one, is given by the following set of reaction equations

$$Au_2^+ + CH_4 \rightleftarrows Au_2(CH_4)^+ \quad (1)$$

$$Au_2(CH_4)^+ + CH_4 \rightarrow Au_2(CH_4)_2^+ \quad (2)$$

$$Au_2(CH_4)_2^+ + O_2 \rightarrow Au_2(CH_4)_2O_2^+ \quad (3)$$

$$Au_2(CH_4)_2O_2^+ + O_2 + CH_4 \rightarrow Au_2(C_3H_8O_2)^+ + 2H_2O \quad (4)$$

$$Au_2(C_3H_8O_2)^+ \rightarrow Au_2(CH_4)^+ + 2CH_2O \quad (5)$$

The fit of the integrated rate equations of this mechanism is represented by the solid lines in Figure 1b, and it is found to be in excellent agreement with the experimental data.

The reversible adsorption of one methane molecule to Au_2^+ (eq 1) describes the first reaction step. This equilibrium reaction is not part of the actual catalytic cycle. $Au_2(CH_4)^+$ is only observed in the experiment at higher temperatures because the subsequent attachment of a second methane molecule (eq 2) is too fast compared to the time resolution of the experiment to be detected at 210 K. The formation of $Au_2(CH_4)_2^+$ then enables the cooperative coadsorption of molecular oxygen, yielding the products $Au_2(CH_4)_2O_2^+$ and $Au_2(C_3H_8O_2)^+$ (eq 3 and 4). The theoretical simulations indicate the liberation of water and hydrogen molecules in this last reaction step. The catalytic cycle is closed by the reformation of the initial product $Au_2(CH_4)^+$ upon the release of two formaldehyde molecules.

An alternative mechanism, in which Au_2^+ would be included in the reaction cycle, is clearly inadequate because the resulting fit does not even lead to a qualitative agreement with the measured data. On the basis of the mass spectrometric and reaction kinetic data, the catalytic cycle might also be closed by the reformation of $Au_2(CH_4)_2^+$ in eq 5 leading to the release of one CO_2 molecule. Yet, such a mechanism can be ruled out based on our theoretical simulations. Another alternative reaction mechanism would involve the generation of $Au_2(C_3H_8O_2)^+$ by coadsorption of molecular oxygen to $Au_2(C_2H_4)(CH_4)^+$. However, the formation of ethylene, C_2H_4, is only observed at elevated temperatures (due to the high activation barriers involved, see below) at which oxygen desorbs and is thus excluded from appearing as a ligand in the complex $Au_2(C_3H_8O_2)^+$.

It should be emphasized that the cooperative action of multiple molecules is essential for the catalytic reaction cycle. Thus, the adsorption and activation of O_2 on the gold dimer cation is found to require preadsorption of methane. In addition, we note the cooperative nature of the C−H bond activation process, requiring the coadsorption of at least two methane molecules on the Au_2^+ cluster; see the Theoretical Results section below.

At a reaction temperature of 240 K (mass spectrum c in Figure 1) the same products as those found at 210 K are observed, albeit in lower abundances. In addition, the product of eq 1, $Au_2(CH_4)^+$ (marked by the green triangle in Figure 1c), can be seen in the mass spectrum, and the $Au_2(CH_4)_2^+$ peak only represents a shoulder of a larger signal at 422 amu, which corresponds to $Au_2(C_2H_4)^+$ (red diamond) containing two dehydrogenated methane molecules. The corresponding kinetic traces are displayed in Figure 1d. At this temperature, about two seconds are required to establish equilibrium concentrations (represented by the constant nonvanishing product signals) under the given partial pressure conditions.

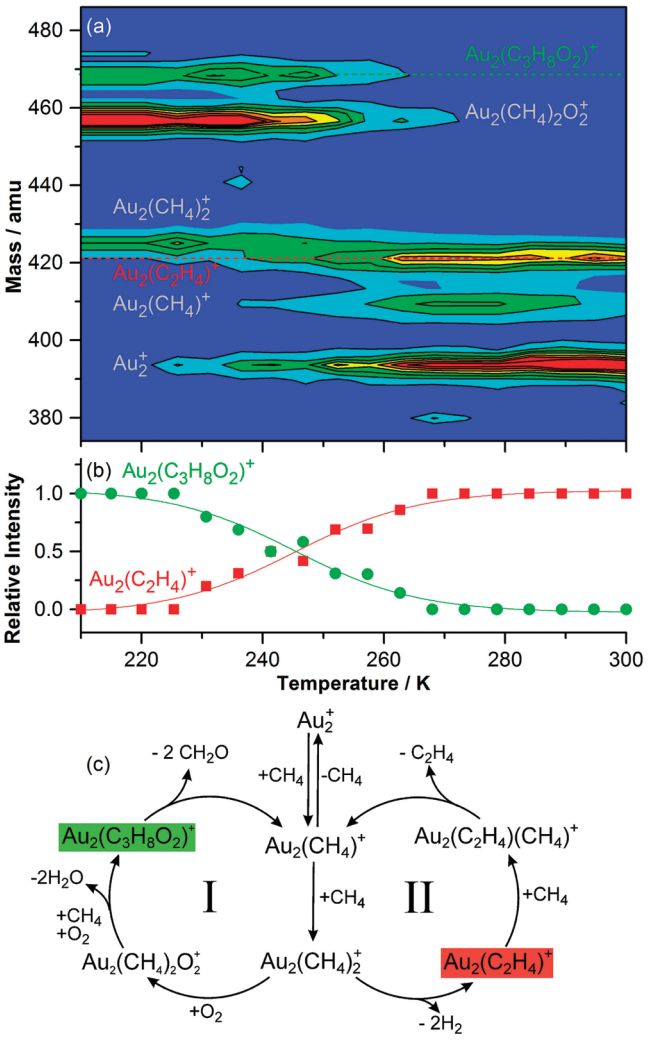

Figure 2. (a) 2D contour plot of the temperature-dependent product ion mass distributions after trapping Au_2^+ for 0.1 s in the presence of $p(CH_4)$ = 0.05 Pa and $p(O_2)$ = 0.10 Pa (one mass spectrum was recorded every 5−6 K; the relative ion intensity is color coded ranging from 0% (blue) to 100% (red)). (b) Relative intensity of the products $Au_2(C_2H_4)^+$ and $Au_2C_3H_8O_2^+$ as a function of the temperature. (c) Proposed reaction mechanism based on the theoretical first-principle calculations yielding the best fit of the experimental kinetic data. The low temperature formaldehyde formation cycle is denoted by I, while II marks the catalytic ethylene generation cycle operative at higher temperatures.

The decrease of the reaction rates with increasing temperature is characteristic for low pressure gas-phase reactions because the primary adsorption reactions of methane and oxygen, respectively, occur without an activation barrier and follow the Lindemann energy transfer model for association reactions.[19,20] In this model the overall reaction rate is largely determined by the stabilizing third-body collisions with helium that occur after the initial cluster−molecule complex formation, and such stabilizing collisions are much more effective at lower temperatures. In addition, the weaker the ligand binding energy, the shorter lived

dx.doi.org/10.1021/jp200160r |J. Phys. Chem. C 2011, 115, 6788–6795

the initial cluster−molecule complex will be and with it the more unlikely its effective stabilization. As a result, molecular oxygen desorbs from the gold cluster complexes above about 250 K because it is only very weakly bound as discussed above.

Nevertheless, at temperatures around 250 K and above, methane still adsorbs on Au_2^+ and is dehydrogenated. Due to the available thermal energy, the apparently activated formation of the new product $Au_2(C_2H_4)^+$ (red diamond) is now possible. Indeed, the latter is the sole product ion (apart from $Au_2(CH_4)^+$ (green triangle)) seen in the mass spectrum recorded at room temperature (Figure 1e). The corresponding kinetic traces at this temperature can be perfectly fitted by a catalytic cycle, in which two methane molecules are cooperatively activated, dehydrogenated, and subsequently reacted to form ethylene

$$Au_2^+ + CH_4 \rightleftarrows Au_2(CH_4)^+ \quad (6)$$

$$Au_2(CH_4)^+ + CH_4 \rightarrow Au_2(CH_4)_2^+ \quad (7)$$

$$Au_2(CH_4)_2^+ \rightarrow Au_2(C_2H_4)^+ + 2H_2 \quad (8)$$

$$Au_2(C_2H_4)^+ + CH_4 \rightarrow Au_2(C_2H_4)(CH_4)^+ \quad (9)$$

$$Au_2(C_2H_4)(CH_4)^+ \rightarrow Au_2(CH_4)^+ + C_2H_4 \quad (10)$$

The fit of the respective integrated rate equations is reflected by the solid lines in Figure 1f.

The same catalytic reaction cycle has been found previously to proceed around room temperature, if only CH_4 was present in the ion trap.[6] Methane is cooperatively activated by the adsorption of a second CH_4 ligand onto $Au_2(CH_4)^+$ (eq 7) leading to dehydrogenation (eq 8). However, the dehydrogenation and condensation product ethylene can only be liberated through the adsorption of a third methane molecule (eq 9) which results in a weakening of the ethylene binding to the complex and the closure of the catalytic cycle via reformation of $Au_2(CH_4)^+$.

The kinetic data obtained at the intermediate temperature of 240 K (Figure 1d) can be fitted by the combination of both catalytic reaction cycles. This fit is of slightly lower quality (particularly for times smaller than 0.6 s) than the ones at the other temperatures (compare with Figure 1b and 1f), and since it could not be improved by consideration of alternative reaction mechanisms we conclude that it is likely that it has been affected by difficulties of the fitting algorithm to handle such a complex reaction mechanism.

The striking temperature dependence of the product mass spectra becomes even more apparent from the 2D contour representation of the temperature-dependent mass spectra displayed in Figure 2a. The oxygen-containing products $Au_2(CH_4)_2O_2^+$ and $Au_2(C_3H_8O_2)^+$ solely appear at low temperatures, whereas the pure hydrocarbon complex $Au_2(C_2H_4)^+$ is only present above 250 K. The two products that contain activated and dehydrogenated methane, $Au_2(C_2H_4)^+$ and $Au_2(C_3H_8O_2)^+$, are highlighted by red and green dashed lines, respectively. The relative intensities of these particular complexes are also shown in Figure 2b illustrating the crossover of the two product formation mechanisms around 250 K. The two catalytic cycles operative at the two temperature regimes (low and high temperature, eqs 1−5 and 6−10, respectively) and their combination, with the latter considered in our analysis of the kinetic data for the intermediate temperature range (around 230−270 K), are depicted in Figure 2c. Hence, the selectivity of the catalytic reaction process, that is, the formation of either formaldehyde (at low temperature) or ethylene (at high temperature), can be controlled by proper tuning of the reaction temperature.

3.2. Theoretical Results. As mentioned above, the analysis of the kinetic data leading to the formulation of the reaction schemes (see eqs 1−10 and Figure 2c) was guided by first-principles density-functional theoretical calculations (see Computational Methods section) which in addition provided deep insights into the nature of bonding of the reactant molecules and reaction intermediates to the gold cluster and revealed the details (pathways and activation barriers) of the reaction mechanism. The reaction profile (RP), along with the calculated atomic structures of the reaction intermediates, transition states (TS), and products, corresponding to the higher temperature catalytic production of ethylene, are shown in Figure 3a and b. The RP and atomic structures corresponding to the low temperature partial oxidation of methane (yielding formaldehyde) are shown in Figure 3c and d.

Both the low and high temperature catalytic cycles start with the adsorption of methane to the gold dimer cation. A methane molecule adsorbs readily to Au_2^+ (adsorption energy E_{ad} = 0.88 eV), with the bonding wave functions formed as superpositions of sp^3 orbitals of the CH_4 molecule with the d-orbitals of the gold cluster; in the lowest energy configuration the methane molecule is bonded directly to one of the Au atoms with two of the H atoms located closer to the gold atom[24] (see structure A (A_0) on the left in Figure 3b (3c)). Adsorption of an additional CH_4 molecule leads to a gain of 0.57 eV, with the optimal bonding configuration marked B (A_1) in Figure 3b (3c), where each of the adsorbed methane molecules is bridged to the nearest gold atom by an H atom.

Cycle I. The sequence of steps denoted by B to T in Figure 3c corresponds to the low temperature cycle (I in Figure 2c), starting with $Au_2(CH_4)_2O_2^+$ (marked B in Figure 3c, which follows the preadsorption of at least one methane molecule) and leading to formation of two formaldehydes and a methane molecule adsorbed on the gold dimer cation ($Au_2(CH_2O)_2CH_4^+$, T in Figure 3c, corresponding to $Au_2(C_3H_8O_2)^+$ in cycle I; see Figure 2c). The binding energy of the adsorbed oxygen molecule to the $Au_2(CH_4)_2O_2^+$ cluster is 0.47 eV, and the activated nature of the adsorbed molecule is portrayed by the increased bond length d(O−O) = 1.29 Å (compared to 1.25 Å in the free O_2 molecule as well as in $Au_2O_2^+$ and 1.26 Å in $Au_2CH_4O_2^+$). The activation of the molecule reflects increased occupation of the nonbonding $2\pi^*$ spin−orbital (SO) component on the adsorbed molecule, occurring via donation of electronic charge from the gold cluster to the adsorbed molecule (which weakens the O−O bond). Using an estimator developed in ref 7 (see the definition of $S(2\pi^*)$ in eqs 5a and 5b of ref 7), we calculate for $Au_2(CH_4)_2O_2^+$ an increased occupancy in the amount of $\Delta S_\downarrow(2\pi^*)$ = 0.35, relative to the free (paramagnetic) oxygen molecule where only the majority-spin nonbonding $2\pi^*$ SO is occupied $S_\uparrow(2\pi^*) = 2$, and therefore $S_\downarrow(2\pi^*) = 0$. The relatively large occupation for $Au_2(CH_4)_2O_2^+$ should be compared with the very small $\Delta S_\downarrow(2\pi^*)$ values calculated by us for the following systems: (i) the nonactivated $Au_2O_2^+$ with $\Delta S_\downarrow(2\pi^*) = 0.05$, and (ii) the nonactivated $Au_2CH_4O_2^+$ cluster, with $\Delta S_\downarrow(2\pi^*) = 0.09$. From all the occupied Kohn−Sham (KS) orbitals of the $Au_2(CH_4)_2O_2^+$ cluster, the highest occupied KS (HOKS) one (see inset marked B in Figure 3c and also the right-hand side of Figure 4) is found to have the largest overlap with the nonbonding $2\pi^*$ orbital (with the appropriate symmetry) of the free O_2

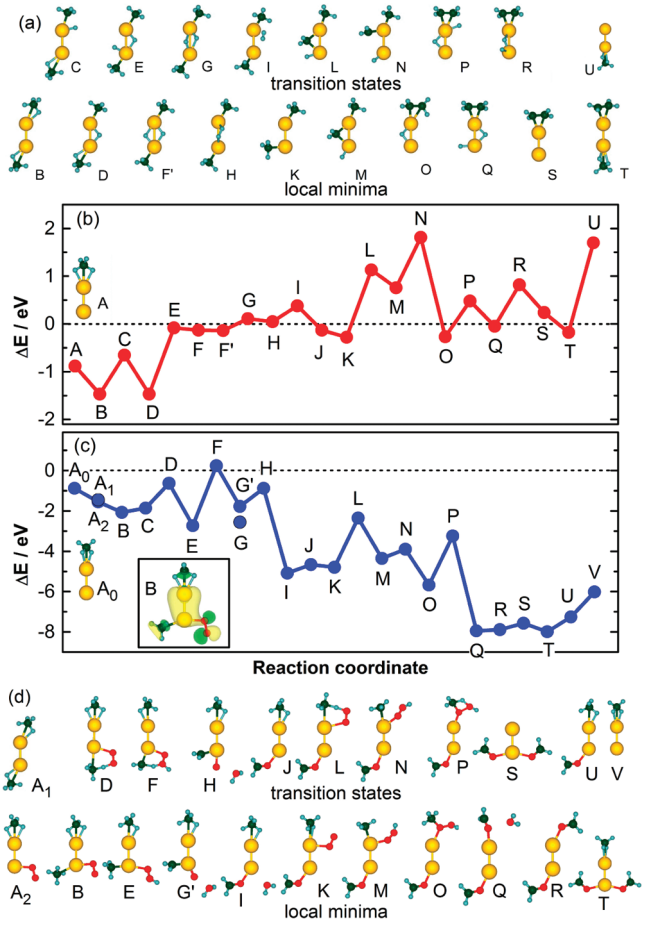

Figure 3. (a) Structures of local minima (lower row) and transition states (upper row) for the ethylene formation cycle; eqs 6−10, cycle II in Figure 2c. (b) Energies of the molecular configurations along the reaction coordinate for the ethylene formation cycle operative above about 250 K. $\Delta E = E(\text{complex}) - \{E(Au_2^+) + nE(CH_4)\} + mE(H_2)$; for configuration U one should add to the right-hand side $E(C_2H_4)$. (c) Energies of the molecular configurations along the reaction coordinate for the formaldehyde formation cycle operative below about 250 K. $\Delta E = E(\text{complex}) - \{E(Au_2^+) + nE(CH_4) + mE(O_2)\} + kE(H_2O)$; for configurations U and V one should add to the right-hand side $E(CH_2O)$ and $2E(CH_2O)$, respectively. Inset: Iso-surface (encompassing 80% of the wave function amplitude) of the minority-spin highest occupied Kohn−Sham (HOKS) orbital of the $Au_2(CH_4)_2O_2^+$ cluster (superimposed on the atomic configuration of the cluster, marked B); light green and yellow colored surfaces correspond to positive and negative signs of the wave function. The $2\pi^*$-like nonbonding nature of the HOKS orbital component on the adsorbed oxygen atoms (red spheres) is apparent from its nodal structure. Note also the s-like (nodeless) nature of the HOKS orbital on the gold (yellow spheres) part of the cluster. (d) Structures of local minima (lower row) and transition states (upper row) for the formaldehyde formation cycle; eqs 1−5, cycle I in Figure 2c. (a) and (b) have been adapted from ref 6. All the species found in the mass spectra (Figure 1), and occurring in the reaction mechanism cycles (Figure 2c), are found on the calculated reaction path (b and c). In (a) and (d) gold atoms are depicted by larger (yellow) spheres, and oxygen atoms are given as smaller red spheres. Carbon atoms are represented by small (green) spheres, and the hydrogen atoms are given by the smallest (light blue) spheres.

molecule (note the nonbonding nodal pattern on the adsorbed O_2). For completeness we display in Figure 4 the iso-surfaces of the HOKS orbitals for: $Au_2O_2^+$ (0.05), $Au_2CH_4O_2^+$ (0.09), and

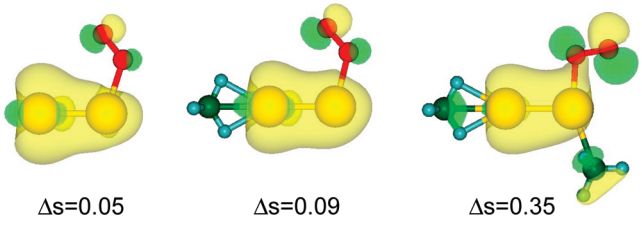

Figure 4. Iso-surfaces (encompassing 80% of the wave function amplitude) of the minority-spin highest occupied Kohn−Sham (HOKS) spin−orbital of the following clusters (from left to right): $Au_2O_2^+$ with $\Delta S_\downarrow(2\pi^*) = 0.05$, $Au_2CH_4O_2^+$ (configuration A_2 in Figure 3d) with $\Delta S_\downarrow(2\pi^*) = 0.09$, and $Au_2(CH_4)_2O_2^+$ (configuration B in Figure 3d) with $\Delta S_\downarrow(2\pi^*) = 0.35$. The iso-surfaces are superimposed on the corresponding atomic configurations. Light green and yellow colored surfaces correspond to positive and negative signs of the wave function. The $2\pi^*$-like nonbonding nature of the HOKS orbital component on the adsorbed oxygen atoms (red spheres) is apparent from its nodal structure. Note also the s-like (nodeless) nature of the HOKS orbital on the gold (yellow spheres) part of the cluster.

$Au_2(CH_4)_2O_2^+$ (0.35), from left to right, respectively; the values in parentheses are the aforementioned $\Delta S_\downarrow(2\pi^*)$ occupations. Comparison of these iso-surfaces illustrates the changes in the nonbonding $2\pi^*$ orbital of the adsorbed oxygen molecule, associated with its increasing occupation occurring upon coadsorption of methane to the gold dimer cation.

The sequence of steps describing the RP in Figure 3c consists of local potential energy minima connected by transition state (TS) barriers. Catalyzed partial oxidation of the adsorbed methanes into formaldehyde molecules occurs through two consecutive multistep processes, B−J and K−R, which are similar to each other, each involving the elimination of a water molecule. The H_2O elimination occurs through activated formation of a hydroperoxo group (−OOH, E in Figure 3d) in a process that involves stripping a hydrogen atom from the methane molecule proximal to the adsorbed oxygen molecule (see B → D → E in Figure 3c and 3d); a subsequent activated H-atom stripping process, E → F → G′, leads to water elimination coupled with oxygen atom insertion into the H_2C−Au−bond resulting in formation of an adsorbed formaldehyde (G′ → H → I → J, with J corresponding to $[H_2CO{-}Au{-}Au{-}CH_4]^+$); note the large energy release accompanying the formaldehyde formation steps [H → I (4.21 eV) and similarly P → Q (4.71 eV)].

Formation of the two formaldehyde molecules, each on one end of the gold dimer (see R in Figure 3d) is followed by a readily occurring translocation ("shuttle") of one of the molecules (R→ S) which frees one of the gold atoms for the adsorption of another methane molecule (S → T), thus forming the observed complex $Au_2(CH_2O)_2CH_4^+$ which appears as a local potential energy minimum (T) on the reaction path. Subsequent activated sequential desorption processes of the two formaldehydes (T → U and U→ V) returns the cycle to the starting stoichiometry, i.e., $Au_2CH_4^+$ (V and A_0), with a net exothermicity of ∼5.0 eV.

Cycle II. Guided by the experimental data where no oxygen-containing species were detected at higher temperature (see, e.g., Figure 1e), we start the discussion of the RP corresponding to cycle II with $Au_2(CH_4)_2^+$ (B in Figure 3a and b). The RP displayed in Figure 3b entails the elimination of two H_2 molecules, resulting in the formation of an ethylene molecule adsorbed on the gold cluster $(Au_2(C_2H_4)^+$, S in Figure 3a and b),

dx.doi.org/10.1021/jp200160r |J. Phys. Chem. C 2011, 115, 6788–6795

corresponding to the bottom right of reaction cycle II (Figure 2c); the same RP has been applied previously[6] in analysis of the reaction of methane with gold dimer cations in the absence of oxygen. The TS encountered in the process of elimination of the first H_2 molecule is given by configuration I, and the subsequent local minimum corresponding to $Au_2(CH_3)_2^+$ is denoted by K. The second H_2 elimination TS barrier is denoted by R. The largest TS barriers in the RP leading to configuration S involve formation of "Au-insertion configurations" where a Au atom is inserted between a CH_3 group and an H atom (not bonded directly to the CH_3 group, see D, F′, and L), as well as translocation of a CH_2 group from one Au atom to another (see the transitions K → L → M → N). Interestingly, direct desorption of ethylene from the complex $Au_2(C_2H_4)^+$ is calculated to be nonfeasible (requiring a very large activation energy). Instead, it proceeds via an intermediate where a CH_4 molecule adsorbs first on the "unoccupied" Au atom $(Au_2(C_2H_4)(CH_4)^+$, configuration T, see also top right of cycle II, Figure 2c) with subsequent desorption of C_2H_4 ending at the start of the cycle (configuration U, compare with Figure 2c).

4. DISCUSSION

The main findings of our investigations pertain to the temperature-controlled selectivity of the reaction processes of methane catalyzed by free Au_2^+ clusters. The mechanisms that we have formulated through reaction kinetics measurements and first-principles calculations are summarized by the two catalytic cycles shown in Figure 2c, in conjunction with the reaction profiles displayed in Figure 3. The catalytic processes portrayed by the two catalytic reaction cycles can be discussed by considering the energies of the molecular complexes calculated along the reaction coordinate (Figure 3). While the largest energy barriers (up to 1.41 eV) for the individual reaction steps in the ethylene cycle (eqs 6−10; cycle II, Figure 3b) are considerably smaller compared to those (up to 2.98 eV) in the formaldehyde cycle (eqs 1−5, cycle I, Figure 3c), the largest (positive) energy difference of any reaction intermediate along the RP with respect to the initial reactants is only 0.24 eV for the formaldehyde cycle (i.e., ΔE for structure F in Figure 3c), compared to a much larger value for the ethylene cycle (i.e., ΔE = 1.81 eV for structure N in Figure 3); positive ΔE values correspond to intermediate reaction complexes which are unstable (that is, characterized by having excess energy) with reference to the initial reactants. Additionally, inspection of the reaction profiles in Figure 3b and c reveals that significantly more energy is released into the gold complex in the formaldehyde cycle (max. 8.00 eV) than in the ethylene cycle (max. 1.47 eV).

Since the experiment is operated in the low pressure multicollision regime[15,25] which does not provide strict canonical (constant temperature) conditions, the discussion of the reaction mechanism should not focus solely on the energy barriers for individual reaction steps, but rather on their combination with the energy gain and the largest excess energy differences (with respect to the initial reactants) along the RP. Under the present low pressure conditions, the estimated rate of thermalizing (stabilizing) collisions is rather slow, $\sim 10^5$ s^{-1}. Consequently, energy that may be gained in certain reaction steps could reside (that is, stored) in the Au_2^+ reaction complex for a sufficiently long time and be used to facilitate passage over activation energy barriers encountered later along the reaction path (akin to microcanonical, i.e., constant energy, conditions). The large energy gain incurred in the formaldehyde cycle makes it most probable that individual energy barriers along the RP would be readily overcome. Furthermore, the rather small excess energy (0.24 eV with respect to the initial reactants) encountered in this reaction implies that the supply of a very small amount of energy (via collisions with the helium buffer gas) would be sufficient for the reaction to occur.

In contrast, in the ethylene cycle the largest excess energy difference encountered along the RP (with respect to the initial reactants) is much higher (1.81 eV), thus requiring a larger energy supply by thermal collisions. Since energy transfer becomes inefficient as the temperature decreases, the ethylene formation reaction is rendered less effective at lower temperature, and it may be utterly inhibited at low enough temperatures. As a result, the ethylene formation cycle is operative at room (and intermediate) temperature, with the formaldehyde cycle dominating at low temperatures (Figure 2b).

The above temperature dependence of the energy transfer rate together with the observed absence of adsorbed oxygen on the catalyst at higher temperatures underlie the observed temperature-controlled selectivity (i.e., low temperature methane partial oxidation versus higher temperature ethylene production, see Figure 2b) of the two-cycle catalysis of methane on free Au_2^+ clusters (Figure 2c) under low pressure multicollision conditions. These results provide the impetus for further investigations aiming at selective temperature control of multicycle catalytic reactions via tuning of adsorption affinities (and activation characteristics) of the reactants (and/or reaction intermediates) through specific selection (tailoring) of the cluster size, elemental composition, and stoichiometry (i.e., alloying) of the nanocatalyst.

AUTHOR INFORMATION

Corresponding Author

*Fax: 404-894-7747. E-mail: uzi.landman@physics.gatech.edu.

ACKNOWLEDGMENT

The experimental work presented was supported by the Deutsche Forschungsgemeinschaft (DFG) and the Fonds der Chemischen Industrie (FCI). In particular, SML is grateful for a Kekulé fellowship of the FCI. The theoretical work (UL and RNB) was supported by the USA Air Force Office for Scientific Research Grant FA9550-08-1-0323.

REFERENCES

(1) Otsuka, K.; Y., W. *Appl. Catal., A* **2001**, *222*, 145.
(2) Crabtree, R. H. *J. Organomet. Chem.* **2004**, *689*, 4083.Olah, G. A.; Goeppert, A.; Prakash, G. K. S. *Beyond Oil and Gas: The Methanol Economy*; Wiley-VCH: Weinheim, 2006. Crabtree, R. H. *Chem. Rev.* **2010**, *110*, 575.
(3) Schröder, D. *Angew. Chem., Int. Ed.* **2010**, *49*, 850.
(4) Schröder, D.; Schwartz, H. *Top Organoment Chem* **2007**, *22*, 1.
(5) Roithova, J.; Schröder, D. *Chem. Rev.* **2010**, *110*, 1170.
(6) Lang, S. M.; Bernhardt, T. M.; Barnett, R. N.; Landman, U. *Angew. Chem., Int. Ed.* **2010**, *49*, 980.
(7) Lang, S. M.; Bernhardt, T. M.; Barnett, R. N.; Yoon, B.; Landman, U. *J. Am. Chem. Soc.* **2009**, *131*, 8939.
(8) Socaciu, L. D.; Hagen, J.; Bernhardt, T. M.; Wöste, L.; Heiz, U.; Häkkinen, H.; Landman, U. *J. Am. Chem. Soc.* **2003**, *125*, 10437.
(9) Schröder, D.; Schwarz, H. *Angew. Chem., Int. Ed.* **1990**, *29*, 1433. Schröder, D.; Schwarz, H.; Clemmer, D. E.; Chen, Y.; Armentrout, P. B.; Baranov, V. I.; Böhme, D. K. *Int. J. Mass Spectrom.* **1997**, *161*, 175.

Kretzschmar, I.; Fiedler, A.; Harvey, J. N.; Schröder, D.; Schwarz, H. *J. Phys. Chem. A* **1997**, *101*, 6252. Feyel, S.; Döbler, J.; Schröder, D.; Sauer, J.; Schwarz, H. *Angew. Chem., Int. Ed.* **2006**, *45*, 4681.

(10) Brönstrup, M.; Schröder, D.; Kretzschmar, I.; Schwarz, H.; Harvey, J. N. *J. Am. Chem. Soc.* **2001**, *123*, 142.

(11) Wesendrup, R.; Schröder, D.; Schwarz, H. *Angew. Chem., Int. Ed.* **1994**, *33*, 1174. Pavlov, M.; Blomberg, M. R. A.; Siegbahn, P. E. M.; Wesendrup, R.; Heinemann, C.; Schwarz, H. *J. Phys. Chem. A* **1997**, *101*, 1567.

(12) Haruta, M. *Nature* **2005**, *437*, 1098.

(13) (a) Valden, M.; Lai, X.; Goodman, D. W. *Science* **1998**, *281*, 1647. (b) Sanchez, A.; Abbet, S.; Heiz, U.; Schneider, W.-D.; Häkkinen, H.; Barnett, R. N.; Landman, U. *J. Phys. Chem. A* **1999**, *103*, 9573.(c) Bond, G. C.; Louis, C.; Thomson, D. T. *Catalysis by Gold*; Imperial College Press: London, 2006. (d) *Nanocatalysis*; Heiz, U.. Landman, U., Eds.; Springer-Verlag: Berlin, 2007.

(14) Wallace, W. T.; Whetten, R. L. *J. Am. Chem. Soc.* **2002**, *124*, 7499. Stolcic, D.; Fischer, M.; Ganteför, G.; Kim, Y. D.; Sun, Q.; Jena, P. *J. Am. Chem. Soc.* **2003**, *125*, 2848. Lyalin, A.; Taketsugu, T. *J. Phys. Chem. Lett.* **2010**, *1*, 1752.

(15) Bernhardt, T. M. *Int. J. Mass Spectrom.* **2005**, *243*, 1.

(16) Keller, R.; Nöhmeier, F.; Spädtke, P.; Schönenberg, M. H. *Vacuum* **1984**, *34*, 31.

(17) Lang, S. M.; Bernhardt, T. M. *Eur. J. Phys. D* **2009**, *52*, 139.

(18) Schumacher, E. *DETMECH - Chemical Reaction Kinetics Software*; University of Bern: Chemistry Department, 2003.

(19) Steinfeld, J. I.; Francisco, J. S.; Hase, W. L. *Chemical Kinetics and Dynamics*, 2nd ed.; Prentice Hall: Upper Saddle River, NJ, 1999.

(20) Bernhardt, T. M.; Hagen, J.; Lang, S. M.; Popolan, D. M.; Socaciu-Siebert, L.; Wöste, L. *J. Phys. Chem. A* **2009**, *113*, 2724.

(21) Barnett, R. N.; Landman, U. *Phys. Rev. B* **1993**, *48*, 2081.

(22) Troullier, N.; Martins, J. L. *Phys. Rev. B* **1991**, *43*, 1993.

(23) Perdew, J. P.; Burke, K.; Ernzerhof, M. *Phys. Rev. Lett.* **1996**, *77*, 3865.

(24) Lang, S.; Bernhardt, T. M.; Barnett, R. N.; Landman, U. *Chem. Phys. Chem.* **2010**, *11*, 1570.

(25) Bernhardt, T. M.; Socaciu-Siebert, L. D.; Hagen, J.; Wöste, L. *Appl. Catal., A* **2005**, *291*, 70.